THE JOURNAL OF BIOLOGICAL CHEMISTRY VOL. 281, NO. 33, pp. 24048–24057, August 18, 2006

Catalytic Mechanism and Structure of Viral Flavin-dependent Thymidylate Synthase ThyX*

Received for publication, January 25, 2006, and in revised form, May 5, 2006 Published, JBC Papers in Press, May 17, 2006, DOI 10.1074/jbc.M600745200

Sébastien Graziani[‡§1], Julie Bernauer[¶1], Stéphane Skouloubris[‖2], Marc Graille[¶], Cong-Zhao Zhou[¶3], Christophe Marchand[¶], Paulette Decottignies[¶], Herman van Tilbeurgh[¶], Hannu Myllykallio[‖2,4], and Ursula Liebl[‡§5]

From the [‡]CNRS, UMR 7645, Laboratory of Optics and Biosciences, Ecole Polytechnique, 91128 Palaiseau, [§]INSERM, U696, 91128 Palaiseau, [‖]INSERM AVENIR Group, Université Paris Sud, Institut de Génétique et Microbiologie-CNRS UMR 8621, 91405 Orsay, and [¶]Institut de Biochimie et de Biophysique Moléculaire et Cellulaire (CNRS-UMR 8619), Université Paris Sud, 91405 Orsay, France

By using biochemical and structural analyses, we have investigated the catalytic mechanism of the recently discovered flavin-dependent thymidylate synthase ThyX from *Paramecium bursaria* chlorella virus-1 (PBCV-1). Site-directed mutagenesis experiments have identified several residues implicated in either NADPH oxidation or deprotonation activity of PBCV-1 ThyX. Chemical modification by diethyl pyrocarbonate and mass spectroscopic analyses identified a histidine residue (His[53]) crucial for NADPH oxidation and located in the vicinity of the redox active N-5 atom of the FAD ring system. Moreover, we observed that the conformation of active site key residues of PBCV-1 ThyX differs from earlier reported ThyX structures, suggesting structural changes during catalysis. Steady-state kinetic analyses support a reaction mechanism where ThyX catalysis proceeds via formation of distinct ternary complexes without formation of a methyl enzyme intermediate.

All cellular organisms need thymidylate (dTMP) for the replication of their chromosomes, as dTMP is required for the biosynthesis of dTTP, a building block of DNA. Cells can produce thymidylate either *de novo* from dUMP or incorporate thymidine using thymidine kinase. The *de novo* pathway of dTMP synthesis requires a specific enzyme, thymidylate synthase, that methylates dUMP at position 5 of the pyrimidine ring. Two structurally and mechanistically distinct classes of thymidylate synthases exist. The well studied ThyA proteins (EC 2.1.1.45) catalyze the reductive methylation reaction of dUMP, with methylenetetrahydrofolate (CH_2H_4folate)[6] serving as one-carbon donor and as source of reductive power (reviewed in Ref. 1).

On the other hand, the recently discovered ThyX (EC 2.1.1.148) family of thymidylate synthases contains FAD (2) that is tightly bound by a novel fold (3). FAD mediates hydride transfer from NADPH during catalysis (4–6). Consequently, in the reaction catalyzed by ThyX, CH_2H_4folate serves only as a carbon donor, leading to the prediction that tetrahydrofolate (and not dihydrofolate as is the case for ThyA) is produced (2). This prediction has recently been confirmed by identifying tetrahydrofolate as a reaction product of *Chlamydia trachomatis* ThyX using high pressure liquid chromatography (7).

The catalytic reaction of thymidylate synthase ThyA is a sequential ordered mechanism in which dUMP binding is followed by the entry of CH_2H_4folate, and subsequent ternary complex formation with dUMP and CH_2H_4folate simultaneously bound to the enzyme (8, 9). This was demonstrated by thorough steady-state kinetic measurements using varying concentrations of these two substrates of the ThyA reaction. Moreover, by using fluoro-dUMP in the reaction mixtures, this covalent ternary complex can readily be trapped for ThyA proteins (10). Although ThyX catalysis is of considerable interest for detecting and designing new anti-microbial compounds (2), our understanding of the reaction mechanism of this enzyme is still incomplete. Several models propose that the catalytic cascade of different ThyX proteins starts with oxidation of NADPH (4–6), a reaction step that does not occur during ThyA catalysis. We have proposed earlier that *Paramecium bursaria* chlorella virus-1 (PBCV-1) ThyX uses a reaction mechanism with the formation of a ternary complex of CH_2H_4folate and dUMP bound to the enzyme (6). This proposal is compatible with a structural model where dUMP and CH_2H_4folate are simultaneously docked at the active site of ThyX from *Thermotoga maritima* (4). However, a ping-pong mechanism involving the formation of a methyl enzyme as a reaction intermediate has been proposed for *C. trachomatis* ThyX proteins (7). Fluoro dUMP does not seem to form a covalent intermediate with ThyX enzymes (11), complicating the analysis of the ThyX reaction. Consequently, it is currently unknown whether this discrepancy results from experimental differences or rather indicates that ThyX proteins from viral and cellular sources might use different reaction mechanisms.

The goal of this work is to obtain detailed insight into the enzymatic mechanism of the highly active PBCV-1 ThyX pro-

* This work was supported in part by a grant from the Programme Microbiologie Fondamentale (to U. L. and H. M.). The costs of publication of this article were defrayed in part by the payment of page charges. This article must therefore be hereby marked "*advertisement*" in accordance with 18 U.S.C. Section 1734 solely to indicate this fact.

[1] Both authors contributed equally to this work.

[2] Supported by INSERM (Bioavenir and Jeune Chercheur Programs) and the Fondation Bettencourt Schuller.

[3] Present address: School of Life Science, University of Science and Technology of China, Hefei Anhui, 230027, China.

[4] To whom correspondence may be addressed. Tel.: 33-1-69-15-81-70; Fax: 33-1-69-15-78-08; E-mail: hannu.myllykallio@igmors.u-psud.fr.

[5] To whom correspondence may be addressed. Tel.: 33-1-69-33-47-40; Fax: 33-1-69-33-30-17; E-mail: ursula.liebl@polytechnique.edu.

[6] The abbreviations used are: CH_2H_4folate, methylenetetrahydrofolate; PBCV-1, *P. bursaria* chlorella virus-1; DEPC, diethylpyrocarbonate; MALDI-TOF MS, matrix-assisted laser desorption ionization-time of flight mass spectrometry; r.m.s.d., root-mean-square distance.

tein using a combination of biochemical and structural approaches. We therefore identified and further investigated several residues required for substrate binding and/or catalysis of PBCV-1 ThyX. Moreover, we report the crystal structure of the PBCV-1 ThyX tetramer that provides a structural basis for the interpretation of the obtained functional data. We observed that the conformation of active site key residues of PBCV-1 ThyX is different from earlier reported ThyX structures, suggesting that the active site undergoes structural changes during catalysis. Our detailed steady-state kinetic analyses continue to indicate that ThyX uses a reaction mechanism where catalysis proceeds via formation of distinct ternary complexes.

EXPERIMENTAL PROCEDURES

Bacterial Strains—The bacterial strains used in this study are *Escherichia coli* BL21 (*F*$^-$ *ompT hsdSB* (r_B^- m_B^-) *gal dcm*; Novagen) and the thymidine auxotroph DH5α (Δ*thyA*::Erm (12)). *E. coli* strains were grown at 37 °C in Luria Bertani or in M9 (Difco) minimal medium (3 g/liter Na_2HPO_4, 1.5 g/liter KH_2PO_4, 0.25 g/liter NH_4Cl, and 0.15 g/liter NaCl) supplemented with 2 mM $MgSO_4$, 0.1 mM $CaCl_2$, and 0.3% glycerol. One hundred μg/ml ampicillin and 1 mM isopropyl β-D-thiogalactopyranoside were added for plasmid maintenance or protein induction, respectively. Complementation tests were performed as described previously (11).

Molecular Genetic Techniques and Construction of Plasmids—The pVEX plasmid containing the *thyX* gene from PBCV-1 is a pGEX-2T derivative that has been described previously (6). Site-directed mutations were introduced using the QuikChange mutagenesis kit (Stratagene) with pVEX (T7tag-a674r6His) as template using the following primer couples (all sequences are indicated in 5′ to 3′ direction): CCACAAGCATGGTCAATC and CATAGGCGGTGTTCGTAACC for H53Q; CCACAAGAAGTGGTCAATC and CATAGGCGGTGTTCTTCACC for H53K; CGCCAGCGGAGCTTCCACTTC and CGAGTCCAAGAAGCGGTCGCC for H79Q; CGCAAGCGGAGCTTCCACTTC and GTCCAAGAAGCGTTCGCCTCG for H79K; CAGGCGTACGCATCTGTGATG and CGTACGCCTGGGAAAATTCCT for R90A; GGATCCAGTACATCGAACTGC and CCCTAACCTAGGTCATGTAGC for H177Q; GGATCAAGTACATCGAACTGC and CCCTAACCTAGTTCATGTAGC for H177K; CGAACTGGCGACTTCAAACGG and GCTTGACCGCTGAAGTTTGCC for R182A. The E190G substitution was obtained as described earlier (6).

Protein Expression and Purification—The PBCV-1 wild-type and mutant ThyX proteins were expressed in either *E. coli* DH5α (Δ*thyA*) or BL21 at 37 °C in 800 ml of LB medium containing 100 μg/ml ampicillin. Protein expression was induced by adding 1 mM isopropyl β-D-thiogalactopyranoside to early exponential phase cultures ($A_{600} \sim 0.5$) for 3 h. His-tagged proteins were purified from cell-free extracts by gravity-flow chromatography on nickel-nitrilotriacetic acid-agarose (Qiagen) and gel filtration using an S-200 column (Amersham Biosciences). Eluted proteins were stored at −80 °C in 50 mM HEPES, pH 7.0, supplemented with 10% glycerol. Protein samples were analyzed on 12.5% SDS-PAGE and were more than 95% pure.

ThyX Activity Measurements—Tritium release assays for measuring PBCV-1 ThyX activity *in vitro* were performed essentially as described earlier for the *Helicobacter pylori* ThyX protein (11) with 37.5 pmol of enzyme in a 25-μl reaction mixture. Reactions were terminated after 3.5 min of incubation. Kinetic parameters were determined using nonlinear regression using the software package GRAPHPAD. Typical reactions contained 10 mM $MgCl_2$, 0.5 mM NADPH, 60 μM FAD, 500 μM CH_2H_4folate, 12.5 μM dUMP, 10% glycerol in 50 mM HEPES, pH 7.5. The specific activity of the [5-^{3}H]dUMP stock (Moravek) used in the experiments was 13.6 Ci/mmol. Activities of mutant proteins analyzed were compared with those of wild-type protein obtained in parallel experiments.

In double titration experiments, the concentrations of dUMP and CH_2H_4folate were varied from 3 to 50 μM and from 3 to 100 μM, respectively; CH_2H_4folate and NADPH were varied from 3 to 100 μM and from 100 to 300 μM respectively, and the concentrations of dUMP and NADPH were varied from 3 to 100 μM and from 6.25–200 μM, respectively. Where indicated, deprotonation assays were also performed using enzyme treated with diethylpyrocarbonate (see below).

NADPH oxidation activity of ThyX proteins was measured using a total volume of 100 μl. Reaction components were 50 μM dUMP, 10% glycerol, 1 mM $MgCl_2$, 400 μM NADPH, 10 μM FAD. Control experiments established that the addition of 50 μM of CH_2H_4folate substantially inhibited NADPH oxidation activity. Activity was monitored by net *decrease* of absorbance at 340 nm using a CARY 50 spectrophotometer (Varian). An extinction coefficient of 6400 cm^{-1} at 340 nm (ϵ_{340}) was used to quantify absorption changes. Note that this assay is different from the spectrophotometric assay established for ThyA proteins that catalyze the oxidation of tetrahydrofolate to dihydrofolate resulting in net *increase* in absorption at 340 nm. Fluorescence detection measurements of oxidation activity were performed at 340 nm excitation and 460 nm emission, using a Chameleon II multilabel plate reader (Hidex Oy, Finland). Under these experimental conditions, nonmodified PBCV-1 enzyme decreased fluorescence intensity 1250 arbitrary units/min (corresponding to 100% indicated in Table 2), whereas the activity of DEPC-treated enzyme was not detectable.

Chemical Modification of PBCV-1 ThyX with DEPC and Reversal of Reaction with Hydroxylamine—DEPC has been used to analyze the functional role of histidine residues in a number of proteins, although under certain conditions nonspecific reactions with serine and threonine residues can occur. In the presence of DEPC, histidine residues yield an *N*-carbethoxyhistidyl derivative that is reversible upon addition of hydroxylamine (NH_2OH). In the experiments shown, DEPC was freshly diluted with absolute ethanol before each use. Its concentration was determined by reaction with imidazole as described (13). Modification of PBCV-1 ThyX was performed at 25 °C for 20 min in 980-μl final volume containing 15 μM PBCV-1 ThyX wild-type protein (15 nmol), 50 mM potassium phosphate buffer, pH 7.0, and 250 μM DEPC (the final concentration of ethanol never exceeded 3% (v/v)). A control experiment was performed under the same conditions without DEPC. 54 μl of 1 M hydroxylamine hydrochloride (adjusted to pH 7.0) was added to 490 μl of DEPC-treated PBCV-1 ThyX wild type

and control solutions, and the reaction was carried out at 25 °C for 20 min. DEPC and hydroxylamine were removed by size exclusion chromatography using a 5-ml Sephadex G-25 desalting column (Amersham Biosciences) equilibrated in 50 mM potassium phosphate buffer, pH 7.0. Samples were routinely concentrated to 80 μl in a Microcon YM10 concentrator (Amicon) before proteolytic digestion and mass spectrometry.

Proteolytic Digestion and MALDI-TOF Mass Spectrometry—1 μl of trypsin (1 mg/ml) was added to 15 μl (~1 nmol) of concentrated control protein and DEPC-inactivated ThyX before and after hydroxylamine treatment. The digestion was carried out for 5 h at 37 °C in 50 mM potassium phosphate buffer, pH 7.0, in a final volume of 25 μl. Peptide mass fingerprints were recorded in reflector positive ion mode (accelerating voltage 20 kV, grid voltage 73%, guide wire 0.002%, delay 200 ns) on a Voyager DE-STR MALDI-TOF mass spectrometer (PerSeptive-Applied Biosystems) equipped with a 337 nm nitrogen laser using a close external calibration covering the range 750–4000 Da. 1 μl of peptide solutions was mixed with 3 μl of 50% acetonitrile, 0.3% trifluoroacetic acid, and 6 μl of saturated solution of μ-cyano-4-hydroxycinnamic acid in 30% acetonitrile, 0.3% trifluoroacetic acid. 1.3 μl of this premix was then deposited onto the sample plate and allowed to dry at room temperature.

Chemicals—CH_2H_4folate was a generous gift of Dr. Moser (Eprova). FAD, dUMP, DEPC, and hydroxylamine were purchased from Sigma.

Crystallization and Structure Determination—Protein samples were stored in 0.1 M Tris-HCl, pH 8.5. Protein crystals were grown at 18 °C from a 1:1 μl mixture of 10 mg/ml protein solution with 10% PEG 400, 0.1 M $MgCl_2$, 18% isopropyl alcohol, and 5% PEG MME 550. The best crystals were obtained for the protein incubated with 1 mM FAD before crystallization. For data collection, crystals were transferred to a cryo-solution consisting of 30% PEG 400, 0.1 M $MgCl_2$, 18% isopropyl alcohol, 5% PEG MME 550 and subsequently flash-cooled in liquid nitrogen. Diffraction data were collected at 100 K on the ID14-EH2 beam line (ESRF, Grenoble, France). These data were processed using XDS package (14). The crystals belong to the $P2_12_12$ space group with predicted two molecules per asymmetric unit and a solvent content of 51%. Molecular replacement was done using the program Molrep (15) and coordinates of the previously solved crystal structure of TSCP (TM0449) from *T. maritima* (Protein Data Bank code 1kq4 (3)). In the resulting model, the two monomers of ThyX had an R_{factor} of 58.8% for data in the 20 to 4 Å range. However, by applying symmetry operations, the biologically active tetramer previously observed for TM0449 is reconstituted (3), indicating that this model is correct. This was further confirmed by automated refinement and rebuilding of the model using the program ARP/wARP (16), which led to automatic construction of 83% of the model and significant improvement of the R_{free}. The structure was refined using the program Refmac (17) and manually rebuilt with Turbo Frodo (18). As some regions were found to adopt different conformations, NCS restraints were not used during refinement. The final model (the intact protein is made of 222 amino acids including the hexahistidine tag) contains residues 1–35, 39–89, and 124–216 for chain A and 1–88 and 125–215 for chain B. In addition, two FAD and 247 water molecules have been built. All these residues are well defined in the $2F_o - F_c$ electron density map and fall within the allowed region of the Ramachandran plot, as defined by Procheck (19). Statistics for data collection and refinement are reported in Table 1.

RESULTS

Structure of PBCV-1 ThyX—The crystal structure of the PBCV-1 ThyX protein complexed to its FAD cofactor was solved by molecular replacement using the *T. maritima* TM0449 structure (hereafter designated TmThyX) as starting model and refined to 2.3 Å resolution. As shown in Fig. 1*A*, the PBCV-1 ThyX monomer adopts the same hammerhead shark-shaped structure as *T. maritima* and *Mycobacterium tuberculosis* ThyX (named MtbThyX) with approximate dimensions $30 \times 35 \times 70$ Å^3 (3, 20). The monomer is made of a central α/β domain consisting of a curved four-stranded anti-parallel β-sheet (β1, β2, β4, and β3) and six helices (α1, α2, α3, α6, α7, and α8) packed against the same face of the sheet. Two additional long α-helices (α4 and α5) form a distinct domain on top of the core. The r.m.s.d. value between PBCV-1 and TmThyX or MtbThyX monomers is 1.5 or 1.95 Å, respectively (values calculated for 160–170 Cα atoms). The differences between these structures reside mainly in small variations in the orientation of the helices that are not in direct contact with the β-sheet of the central core domain (α1, α2, α8, α4, and α5).

Although only two PBCV-1 ThyX monomers (chains A and B) are present in the asymmetric unit (r.m.s.d. between these two chains is 0.27 Å for all main chain atoms), a homotetramer similar to the one described previously for TmThyX and MtbThyX can be obtained by applying the space group symmetry operations (Fig. 1*B*, r.m.s.d. between the tetrameric forms of *T. maritima* and PBCV-1 ThyX is 3.81 Å for Cα atoms only) (3, 20). The homotetramer has approximate dimensions of $50 \times 60 \times 85$ Å^3. As observed previously, the tetramer is mostly formed by stacking of helices from the core domains as well as by pairwise interaction of the long helices α4 and α5 that are detached from the core domain.

FAD Binding Mode—The purified PBCV-1 ThyX protein is characterized by a yellow color, indicating that the oxidized form of the flavin cofactor remains tightly bound to this viral protein during all the purification steps (3, 20). Similarly to other structures of ThyX proteins, the FAD cofactors lie in large clefts at the interface between the four monomers and adopt an elongated conformation. The FAD molecules are deeply buried because only 15% from each FAD molecule surface remains solvent-accessible. This accessible region corresponds to the isoalloxazine (flavin) ring of the FMN moiety where the redox chemistry takes place. On the opposite side of the FAD cofactor, the ribityl and AMP parts are strongly fixed onto the protein and fully buried. Surprisingly, superposition of the *T. maritima* and *M. tuberculosis* structures of flavin-dependent thymidylate synthase ThyX onto the PBCV-1 ThyX-FAD complex shows that the FAD adenosine ring adopts a different conformation in the PBCV-1 enzyme (Fig. 1, *C* and *D*). In PBCV-1 ThyX, two adenosine moieties bound to two distinct monomers are stacked together (mean distance of 3.6 Å between adenosine rings) and sandwiched inbetween two histidine rings

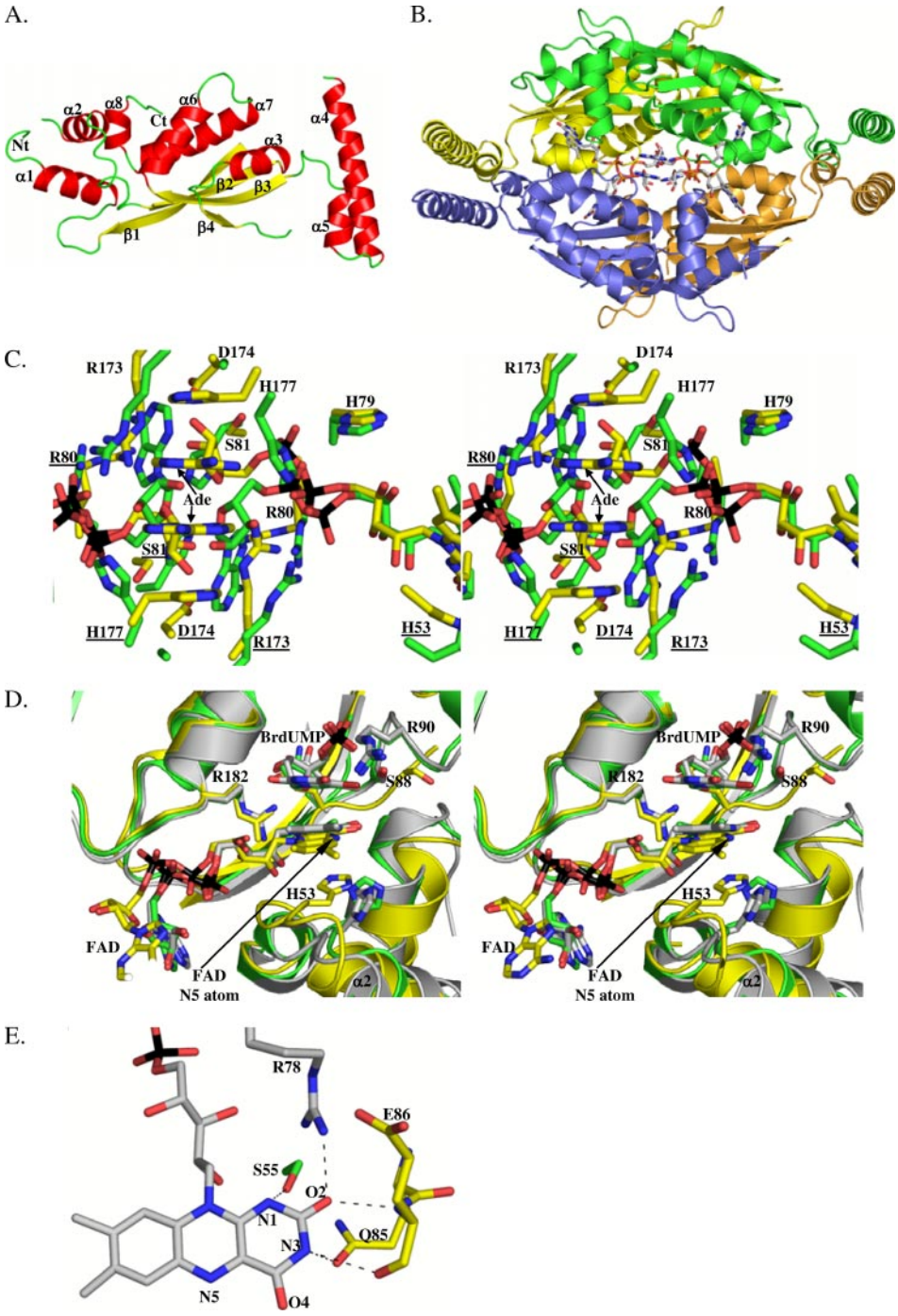

FIGURE 1. **PBCV-1 ThyX structure.** *A,* ribbon representation of the PBCV-1 ThyX monomer. *B,* ribbon representation of the ThyX homotetramer; each monomer is colored differently. The four bound FAD molecules are shown as *sticks.* The monomer highlighted in *green* is related to the representation in *A* by a 90° rotation along the *x* axis. *C,* stereo view representation of the comparison of the ThyX FAD binding mode. PBCV-1 and MtbThyX are colored *yellow* and *green*, respectively. For clarity, only PBCV-1 ThyX numbering is indicated. As TmThyX FAD binding mode is closely similar to that of MtbThyX, it has been omitted. Phosphorous atoms from FAD are colored *black.* For clarity, the labels corresponding to residues from monomer B are *underlined. D,* stereo view representation of the superposition of the active sites from PBCV-1 (*yellow*), MtbThyX (*green*), and TmThyX (*gray*). For clarity, only PBCV-1 ThyX numbering is indicated. Phosphorous atoms from FAD are colored *black. E,* ribbon representation of the hydrogen bonding pattern responsible for the binding of the FAD isoalloxazine moiety. Residues from monomers A, A′, and B are colored *gray, yellow,* and *green,* respectively.

(His^{177} from chain A and B′, distances of 4.1 and 3.5 Å, respectively), thus forming a four-layered ring stack. In Tm- and MtbThyX, the corresponding adenosines point away from each other and lie on the side chain from the residue directly following the RHR signature, His^{98} (MtbThyX) and Ile^{81} (TmThyX). In PBCV-1 ThyX, the pocket that is equivalent to the Mtb- and TmThyX AMP-binding site is blocked by the side chains from His^{83} from monomer A and Glu^{58}, Thr^{171}, Arg^{173}, and Asp^{174} from monomer B. The phosphoribityl binding mode exhibits a high degree of similarity with structures described previously and hence will not be described here. The tricyclic isoalloxazine carries the reactive moiety of FAD. In the absence of bound dUMP, the isoalloxazine ring in PBCV-1 ThyX is solvent-accessible on its *si*-face, and the *re*-face packs onto the His^{53} side chain, involving this residue in hydrophobic packing interactions. In the Mtb- and TmThyX structures, the ring of the corresponding histidine and the isoalloxazine ring are not stacked but bound in a perpendicular direction at the edge of this ring. Comparison of the residues homologous to His^{53} in these three enzymes shows that in PBCV-1 ThyX, helix α2, which precedes the loop bearing His^{53}, has slipped along the helical axis by about 2.7 Å, resulting in a more buried position for His^{53} (Fig. 1*D*).

In addition, the isoalloxazine pyrimidine ring makes five hydrogen bonds with residues originating from three different monomers (A, A′, and B′). The interaction of the N-η1 atom from the invariant Arg^{78} residue (corresponding to the first arginine residue of the RHR sequence motif, characteristic of ThyX proteins) with the O-2 atom of the FAD molecule is of interest from a catalytic point of view. The presence of a largely conserved and positively charged residue near this part of the FAD was suggested to be functionally relevant either in modulating the redox potential of the cofactor or in stabilizing the anionic form of the reduced flavin (21). The four remaining hydrogen bonds are made by the Ser^{55} hydroxyl group (monomer B′) with FAD N-1, the Glu^{86} amide group (monomer A′) with FAD O-2 as well as the Gln^{85} O-ϵ2, and the Glu^{86} carbonyl oxygen (both from monomer A′) with FAD N-3 (Fig. 1*E*).

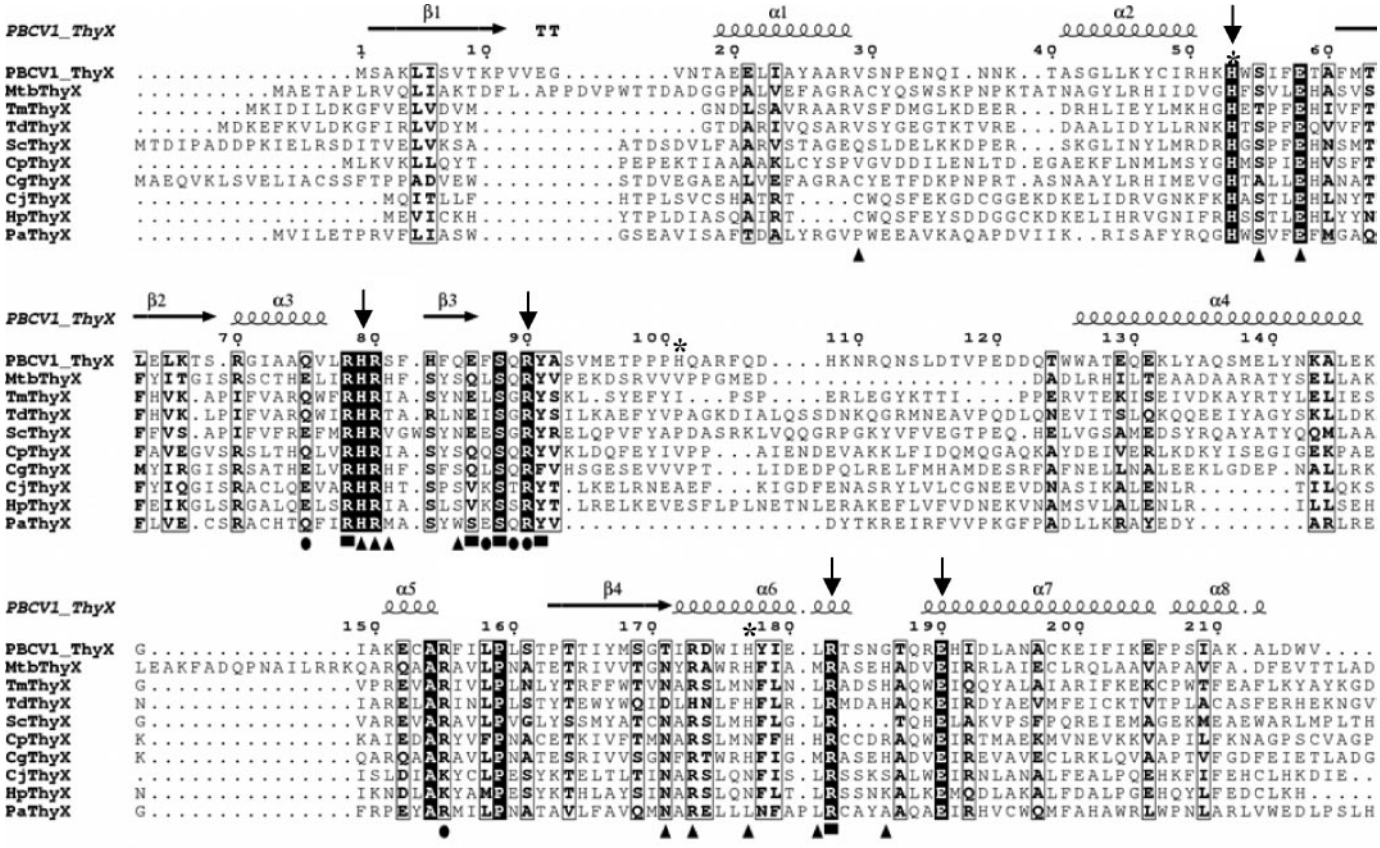

FIGURE 2. **Structure-based sequence alignment of ThyX proteins.** PBCV-1 ThyX secondary structure elements are indicated above the sequence. ThyX positions involved in *T. maritima* ThyX structure, in FAD or dUMP binding, or both are indicated below the sequence by *triangles*, *circles,* or *squares*, respectively. *Arrows* indicate residues investigated in this work using site-directed mutagenesis. *Asterisks* refer to PBCV-1 ThyX histidine residues modified by DEPC. Strictly conserved residues are in *white* on a *black background*. Partially conserved amino acids are *boxed*. This figure was generated using the ESPript program (25). *Td*, *Treponema denticola*; *Sc*, *Streptomyces coelicolor*; *Cp*, *Clostridium perfringens*; *Cg*, *Corynebacterium glutamicum*; *Cj*, *Campylobacter jejuni*; *Hp*, *H. pylori*; *Pa*, *Pyrobaculum aerophilum*.

Identification of Functionally Important ThyX Residues Using a Structure-based Sequence Alignment—To identify functionally important ThyX residues, we first performed a structure-based sequence alignment of a diverse set of ThyX proteins (Fig. 2). A number of conserved ThyX residues have been characterized previously using site-directed mutagenesis approaches (7, 11, 20). For instance, in *H. pylori* ThyX, mutation of the histidine residue equivalent to PBCV-1 ThyX His^{53} results in no detectable activity, although the protein is folded, as it is still able to bind FAD (11). In parallel, Ser^{88} (all residue numbering used hereafter refers to PBCV-1 ThyX) has been proposed to act as the nucleophile in the catalytic reaction, although in the reported ThyX structures this residue is never optimally located for a nucleophilic attack to occur at position 6 of dUMP (3, 20).

Amino acid residues involved in the binding of FAD or dUMP in ThyX have been identified by crystallographic analyses of ternary complexes (Fig. 2, *circles* and *squares*) (3, 20), but little is known about the residues implicated in NADPH or CH_2H_4folate binding.

In this work we analyzed the role of several conserved residues in ThyX catalysis: His^{53}, His^{79}, Arg^{90}, His^{177}, Arg^{182}, and Glu^{190} (indicated by *arrows* in Fig. 2). Except for His^{53}, the role of these residues in ThyX catalysis and/or substrate binding has not been investigated prior to this study.

TABLE 1
Data collection statistics
Values in parentheses are for the highest resolution shell.

Data collection statistics	
Space group	$P2_12_12$
Wavelength	0.933 Å
Unit cell parameters	
a = 69.264 Å	
b = 76.991 Å	
c = 93.437 Å	
$\alpha = 90° \beta = 90° \gamma = 90°$	
Resolution	20.0-2.3 Å
No. of reflections	109,258
No. of unique reflections	22,844
Multiplicity	4.8
R_{sym}[a] (%)	9.1 (32.7)
Completeness (%)	99.2 (97.4)
$I/\sigma(I)$	14.1 (5.9)
Refinement statistics	
Reflections (working/test)	21,351/1121
R/R_{free} (%)[b]	21.3/26.2
Non-hydrogens atoms	3200
R.m.s.d. bonds (Å)	0.010
R.m.s.d. angles (°)	1.310
Mean B-factor (Å^2)	43.050
Ramachandran plot	
Most favored	91.4%
Allowed	8.6%

[a] $R_{sym} = \Sigma_h\Sigma_i|I_{hi} - \langle I_h\rangle|/\Sigma_h\Sigma_i I_{hi}$, where I_{hi} is the ith observation of the reflection h, and $\langle I_h\rangle$ is the mean intensity of reflection h.
[b] $R_{factor} = \Sigma||F_o| - |F_c||/|F_o|$. R_{free} was calculated with a small fraction (5%) of randomly selected reflections.

TABLE 2

Biochemical analyses of the PBCV-1 ThyX mutant proteins

For the oxidation test, 100% (1.56 pmol/min NADPH oxidized) corresponds to the level of activity measured for wild-type protein in the presence of 200 μM NADPH, 1 mM $MgCl_2$, 10% glycerol, 50 μM dUMP, 10 μM FAD together with 0.17 μM enzyme. CH_2H_4folate was found to inhibit oxidation activity and was not included in reaction mixtures for oxidation tests. Deprotonation activities were measured as described under "Experimental Procedures." ND, not determined; −, not detected (less than 3% of the value observed for the wild-type protein).

Substitution	Complementation	Oxidation activity	Deprotonation activity k_{cat} (min^{-1})/(k_{cat}/K_m) (min^{-1} μM^{-1})		
			dUMP	CH_2H_4folate	NADPH
Wild type	++++	100%	15.2/(0.43)	2.6/(0.11)	2.3/(0.09)
H53Q	− (protein insoluble)	ND	−	−	−
H53K	− (protein insoluble)	ND	−	−	−
H79Q	++	94%	8.4/(0.19)	1.47/(0.05)	3.2/(0.09)
H79K	−	ND	−	−	−
R90A	−	56%	−	−	−
H177Q	++	31%	4.6/(0.09)	1.15/(0.05)	4.3/(0.045)
H177K	−	9.5%	−	−	−
R182A	−	20%	−	−	−
E190G	−	−	−	−	−

Mutational Analysis of Conserved Residues of PBCV-1 ThyX—Several site-directed mutants of the above residues were constructed, and their roles in ThyX catalysis were studied (Table 1). Complementation tests indicated that, with the exception of the H79Q and H177Q substitutions, all mutants analyzed did not confer thymidine-independent growth to an *E. coli* strain lacking thymidylate synthase ThyA, thus emphasizing their importance for ThyX activity. The H53Q and H53K mutant strains did not produce soluble protein for biochemical analyses, and the lack of complementation could simply result from improper folding of the protein. All other mutant proteins produced comparable amounts of soluble protein after induction (data not shown). Therefore, the lack of functional complementation suggests that these residues play important roles in ThyX catalysis and/or substrate binding.

To investigate the biochemical basis for the observed loss of complementation activity, the soluble PBCV-1 mutant proteins were expressed and purified. As expected, the complementing mutant proteins, H79Q and H177Q, were still active in NADPH oxidation and deprotonation assays (Table 2). However, both purified histidine mutants were unstable, and their k_{cat}/K_m values changed simultaneously for all three substrates. This could be explained by the role played by both residues in FAD binding. First, the His^{79} side chain packs against the FAD ribityl part and is also hydrogen-bonded to the phosphate group of the AMP moiety (Fig. 1*C*). Second, as mentioned above, the His^{177} side chain is involved in binding of the FAD adenine base in a four-layer stacking. The R90A mutant has lost 44% of its oxidation activity and shows no measurable deprotonation activity. On the basis of the *T. maritima* ThyX structural data, the region containing Arg^{90} participates in dUMP binding (3). Together with our earlier demonstration that dUMP binding is necessary for NADPH oxidation by PBCV-1 ThyX, this provides a feasible explanation for its decreased oxidation activity. The E190G substitution was capable of binding FAD at a wild-type level, but nevertheless lacked detectable oxidation and deprotonation. On the other hand, the R182A mutant did not copurify with oxidized FAD but was able to oxidize NADPH in the presence of 400 μM FAD. For the corresponding residue in MtbThyX, a role for substrate positioning has been proposed to enable hydride transfer during ThyX catalysis (20). Previously, we have shown qualitatively that CH_2H_4folate inhibits NADPH oxidation activity (6). For the R182A mutant protein, we now

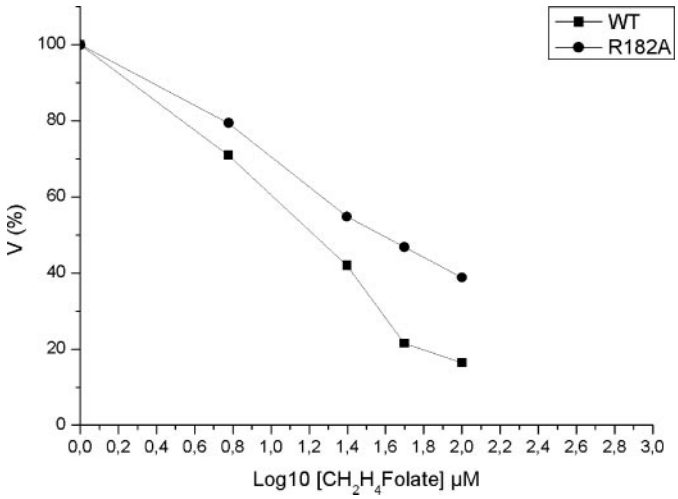

FIGURE 3. **IC_{50} values for CH_2H_4folate, determined for wild type (*WT*) PBCV-1 ThyX (■) and R182A (●).**

determined an IC_{50} value of 48 μM for CH_2H_4folate, whereas the analogous value for the wild type was 16 μM (Fig. 3), indicating that the R182A mutant may affect CH_2H_4folate binding. These results suggest for the first time participation of Arg^{182} in NADPH and/or CH_2H_4folate binding.

ThyX Activity Is Inhibited by DEPC Treatment—As we failed to purify the H53Q and H53K mutant proteins in soluble form, we used chemical modification by DEPC to further investigate the proposed catalytic role(s) of histidine residues (11). For these experiments, the deprotonation activity of PBCV-1 ThyX wild-type protein was measured before and after DEPC treatment. The DEPC treatment decreased ThyX deprotonation activity at least 20-fold and was partially reversible with hydroxylamine (NH_2OH) treatment (see below), indicating that the DEPC-modified histidine residues are implicated in the ThyX catalytic mechanism. More detailed titration experiments with the DEPC-treated enzyme in the presence of varied substrates were performed to further investigate the effect of the chemical modification (Fig. 4, *A–C*). We found that a large, nonphysiological excess of dUMP or CH_2H_4folate still resulted in some detectable deprotonation activity of the chemically modified enzyme, although when NADPH titration was performed, no activity was detected. A possible explanation of this observation is that NADPH, when added after CH_2H_4folate, binds

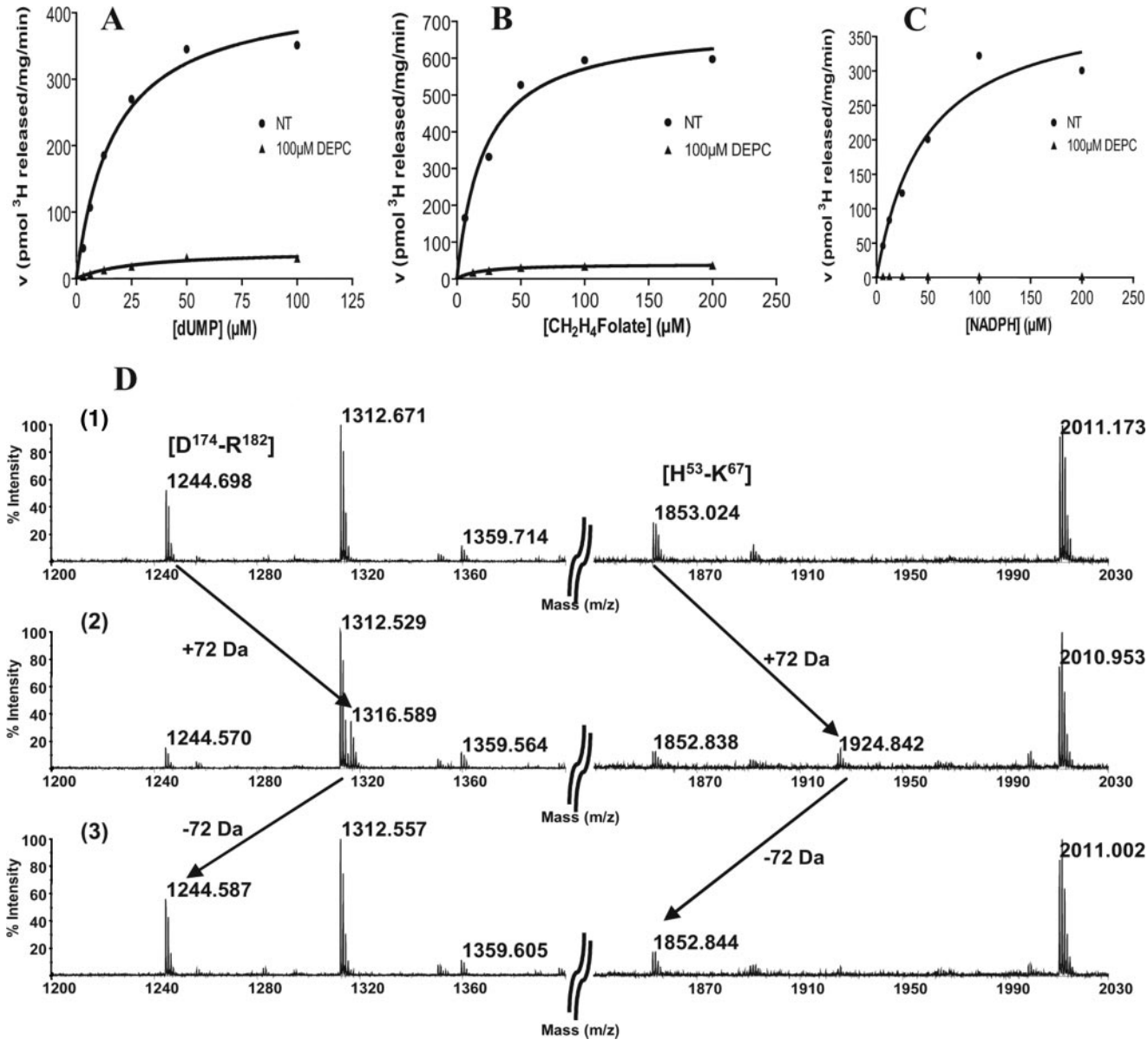

FIGURE 4. **Saturation kinetics of PBCV-1 ThyX with and without DEPC treatment.** Kinetics was determined for dUMP (*A*), CH_2H_4folate (*B*), and NADPH (*C*) in the presence and absence of 100 μM DEPC. Enzyme activity was determined at various concentrations of the indicated substrates, with all other substrates at fixed saturating concentrations as described under "Experimental Procedures." *D* corresponds to the partial MALDI mass spectra (after tryptic digestion) of untreated ThyX (*spectrum 1*), of ThyX after DEPC treatment (*spectrum 2*), and of ThyX after DEPC treatment followed by NH_2OH reversal (*spectrum 3*).

poorly to the chemically modified enzyme. Because of interfering absorbance at 340 nm, oxidation tests could not be performed with DEPC-treated ThyX, but fluorescence detection measurements at 460 nm (after 340 nm excitation) in the presence of 100 μM DEPC revealed no NADPH oxidation activity for the modified enzyme (see "Experimental Procedures" for details).

MALDI-TOF mass spectrometry after tryptic cleavage was performed to identify the modified residue(s). As this derivatization is quite unstable, depending on the conditions (optimum pH 6.0–7.0) (22), all experiments were performed in phosphate buffer, pH 7.0, as quickly as possible, although these conditions were not optimal for trypsin proteolysis and mass spectrometry (no desalting prior to data acquisition). Peptide mass fingerprints clearly showed that three peptides, namely Asp^{174}–Arg^{182}, His^{53}–Lys^{67} (Fig. 4*D*), and Tyr^{94}–Arg^{104} (data not shown), exhibited a 72-Da mass increase after DEPC treatment, in agreement with the derivatization of a histidine residue into carbethoxyhistidine. All of the "fingerprints" contain only one histidine residue, in positions 53, 101, and 177, respectively (modified histidines are indicated in Fig. 2). DEPC has been reported to occasionally react with other nucleophilic groups (principally hydroxyl groups, *e.g.* tyrosine). It has been reported that the effect of DEPC on histidine and tyrosine can be reversed by mild treatment with hydroxylamine, but the reversion is much more rapid in the case of the DEPC-derivatized histidine (13). Thus, to unambiguously assign the mass shift to the specific derivatization of His residues, we have investigated the effect of hydroxylamine on DEPC-treated PBCV-1 ThyX. Fig. 4*D* (*spectrum 3*) shows that the tryptic pro-

file of DEPC-treated PBCV-1 ThyX rapidly returns to the pattern of the control sample after treatment with hydroxylamine. In addition, the mass spectrum of the ThyX protein treated with only hydroxylamine was identical to the one of a control sample (data not shown), indicating that no modification artifact was induced. We can thus conclude that three histidine residues have been modified: His^{53}, His^{101}, and His^{177}. Of these residues, His^{101} is not conserved (Fig. 2), and the H177Q-substituted protein is still functional (Table 2). Therefore, our chemical modification experiments provide further support for a crucial role of His^{53} in NADPH binding and/or oxidation.

Two-substrate Kinetics—To further investigate the kinetic mechanism of PBCV-1 ThyX, we systematically measured deprotonation activity for all possible combinations of the three ThyX substrates, NADPH, dUMP, and CH_2H_4folate, at several fixed concentrations of one substrate while varying the concentration of the second substrate (Fig. 5, *A–C*). For all substrate couples, our data unambiguously demonstrated a set of several converging lines, indicative of a sequential kinetic mechanism, different from what has been reported for *C. trachomatis* ThyX (7). These findings are compatible with our earlier proposal indicating that ThyX catalysis proceeds via formation of ternary complexes of two substrates bound to the enzyme at the same time. Considering that CH_2H_4folate inhibits NADPH binding/oxidation in a competitive way, the binding sites for these two substrates could overlap. Consequently, formation of a quaternary complex where all three substrates are simultaneously bound to the enzyme seems unlikely.

DISCUSSION

To date no structural information is available on the binding modes of ThyX with the substrates NADPH or tetrahydrofolate, and so far our extensive efforts to obtain quality diffracting crystals of PBCV-1 ThyX complexed to its different substrates did not provide exploitable information.

As our kinetic experiments are indicative for simultaneous binding of dUMP and NAD(P)H, we attempted to model the ternary complex with NAD(P)H using the complexes of Tm- and MtbThyX enzymes bound to FAD and dUMP (3, 20) to position dUMP into the active site of PBCV-1 ThyX. As shown in Fig. 2, all residues involved in dUMP binding (*squares* and *circles*) are conserved between PBCV-1, TmThyX, and MtbThyX. Only minor side chain adjustments of residues Glu^{86} and Arg^{155} are needed to accommodate dUMP in the PBCV-1 ThyX active site in the same configuration as for the *T. maritima* and *M. tuberculosis* enzymes. In these complexes the uracil base stacks onto the central ring of the FAD isoalloxazine moiety, and the ribose phosphate is clamped between helix α3 and the substrate binding loop (residues 86–97). In our PBCV-1 ThyX-FAD complex, this loop is mostly disordered, and the hydroxyl group of the putative Ser^{88} catalytic nucleophile (11) is 8–9 Å away from dUMP. In the TmThyX apostructure, this loop is equally unstructured while becoming folded upon interaction with dUMP. Hence, upon substrate binding to PBCV-1 ThyX, this loop could become ordered and bring the Ser^{88} hydroxyl group in closer contact to the substrates.

To fit NADPH into the PBCV-1 ThyX FAD complex, we have searched the Protein Data Bank for all the nonredundant structures describing ternary protein complexes with NAD(P)H and FAD or FMN. We identified 16 of these complexes that could be grouped into three different binding clusters. In the first cluster (grouping nine complexes, best exemplified by glutathione reductase (23)), the nicotinamide ring from the NAD(P)H stacks onto the central isoalloxazine ring in a way that is very similar to the binding mode of dUMP complexed with FAD-ThyX. In the second binding mode (1 complex: 2,4-dienoyl-CoA reductase (24)), the plane of the nicotinamide ring lies perpendicular to the FAD isoalloxazine pyrimidine ring and occupies the same position as the ribose in the dUMP-ThyX complex. In complexes of the third cluster (grouping six cases) FAD (or FMN) is more than 10 Å away from NAD(P)H. None of these modes is fully compatible with our experimental data. However, our biochemical data

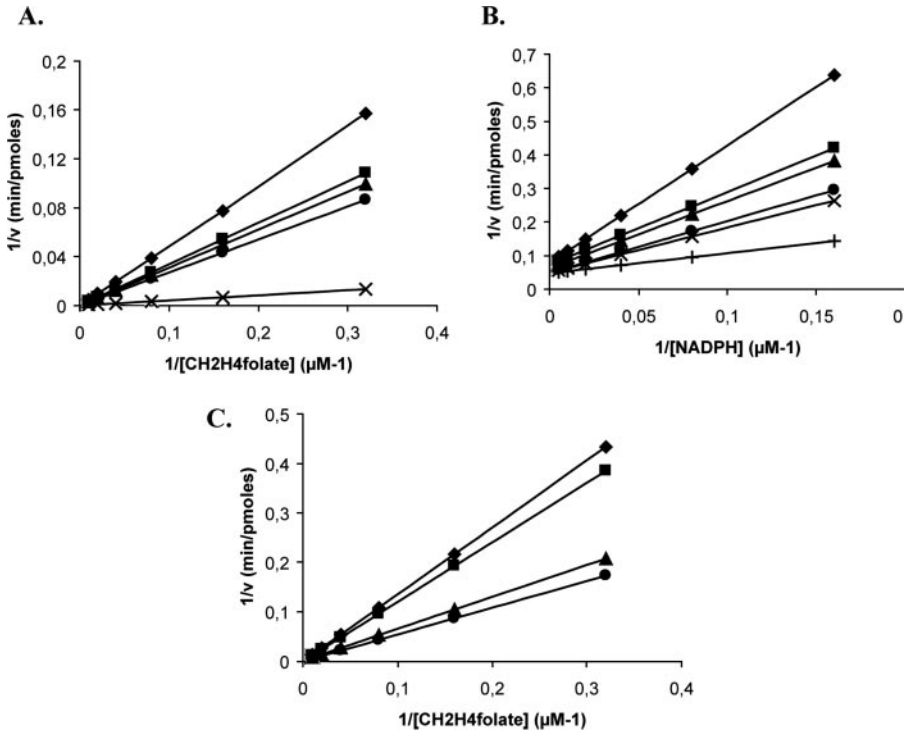

FIGURE 5. **Steady state kinetics of PBCV-1 ThyX catalysis.** Lineweaver-Burk transformation plot corresponding to *A*, titration of CH_2H_4folate with increasing concentrations of dUMP at 50 μM (♦), 25 μM (■), 12.5 μM (▲), 6.25 μM (▲), and 3.125 μM (+). Activity was monitored as release of ^3H from [5-^3H]dUMP, resulting in formation of ^3H_2O. *B*, titration of NADPH using increasing concentrations of dUMP at 100 μM (♦), 50 μM (■), 25 μM (▲), 12.5 μM (▲), 6.25 μM (*), and 3.125 μM (●). *C*, titration of CH_2H_4folate with increasing concentrations of NADPH at 300 μM (♦), 200 μM (■), 150 μM (▲), and 100 μM (●). Values used for linear conversion were obtained by nonlinear regression.

show that NAD(P)H binding and/or oxidation is substantially increased by the presence of dUMP, suggesting that dUMP binding re-orients NADPH at the active site to optimize electron transfer. Structural data with bound NADPH analogs (with or without dUMP) will be required to understand the NADPH binding mode of ThyX proteins.

Our mutagenesis results have identified residues that are important for NAD(P)H oxidation (Table 2). These residues have been mapped in Fig. 6. Apart from His^{53}, mutation of additional ThyX residues provokes moderate (R90A and R182A) to drastic effects (E190G) on NAD(P)H oxidation activity. These three purified mutant proteins still bind FAD, indicating that the tetramer was assembled correctly. In consequence, the loss of NAD(P)H oxidation might either reflect a decreased affinity for NAD(P)H and/or dUMP (the latter being necessary for PBCV-1 ThyX NAD(P)H oxidase activity) or a deleterious effect on catalytic activity. The side chains of the strictly conserved arginine residues at positions 90 and 182 are hydrogen-bonded to the dUMP uracil base. Their substitution by alanine should therefore reduce ThyX affinity for dUMP. The role of Glu^{190} is more complex. In the structures of Tm- and MtbThyX, its carboxylate is hydrogen bonding with Ser^{86} (MtbThyX) or Arg^{105} (TmThyX). It is only poorly solvent-accessible in the ternary ThyX-FAD-dUMP complex and is unlikely to be directly interacting with NAD(P)H. The complete loss of activity of the E190G is probably because of a local destabilization of the active site. Despite their partial NADPH oxidation activity no *in vivo* complemen-tation is observed with the R90A and R182A mutants, because of their lack of protonation activity. From our structural model and in agreement with the proposal of Agrawal *et al.* (4), we conclude that Arg^{90} and Arg^{182} are positioned in a way that they could be involved both in CH_2H_4folate and dUMP binding or methyl transfer to dUMP, explaining why they fail to complement *in vivo*.

The PBCV-1 ThyX H53Q and H53K mutant strains did not produce soluble protein for biochemical analyses, and the lack of complementation could simply result from improper folding of the protein or be due to the more buried position of the histidine side chain (Fig. 1*D*). Site-directed mutagenesis and activity measurements on the corresponding histidine residue in *H. pylori* ThyX (His^{48} (11)) as well as chemical modification studies on PBCV-1 ThyX (Fig. 4*D*) indicate that this histidine side chain has a role in NADPH binding and/or oxidation. This could either be a direct effect or, alternatively, chemical modification of this residue could reorient FAD at the active site influencing NADPH binding. Note also that in Tm- and MtbThyX, the analogous histidine residue is in close vicinity of the redox active N-5 atom of the FAD molecule, suggesting that it could act as proton donor and/or acceptor as observed in most flavin-dependent enzymes (21). In the actual PBCV-1 ThyX structure, His^{53} is not ideally positioned to exert this role. However, His^{53} reacts readily with DEPC, indicating that this residue is accessible and undergoes structural alterations. In agreement with the helix $\alpha 2$ sliding observed between PBCV-1 and Tm- or MtB ThyX structures (Fig. 1*D*), a possible conformational change, possibly induced by substrate binding, might bring the His^{53} N-ϵ2 atom within a more favorable position to abstract (or receive) a proton from the isoalloxazine N-5.

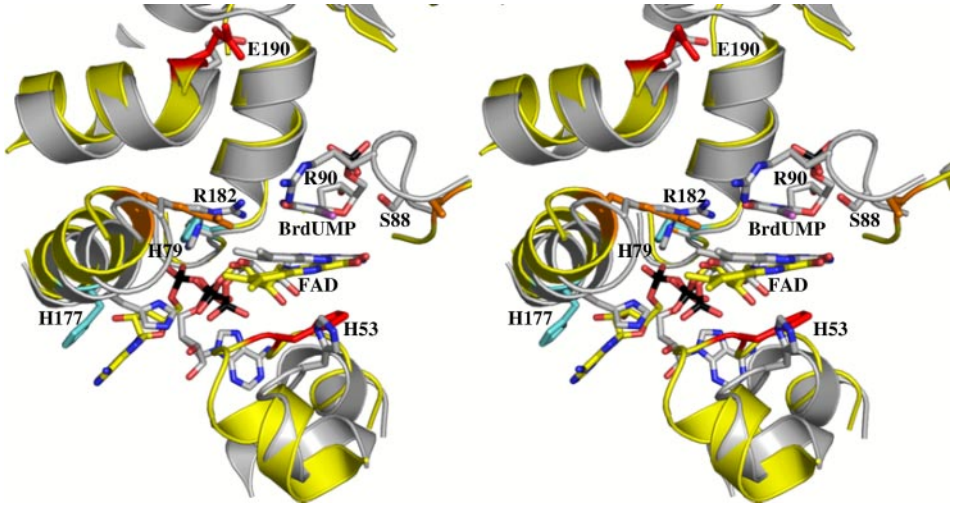

FIGURE 6. **Mapping of the ThyX residues involved in catalysis.** PBCV-1 and MtbThyX are colored *yellow* and *gray*, respectively. PBCV-1 ThyX residues whose mutation completely affects NAD(P)H oxidation or methyl transfer are represented in *red* and *orange*, respectively. The two positions, His^{79} and His^{177} for which substitution by lysine or glutamine has either dramatic or no effect on ThyX activity, are colored in *light blue*. The bromine atom from BrdUMP is colored in *purple*. For clarity, only PBCV-1 ThyX numbering is indicated. Phosphorous atoms from FAD and BrdUMP are colored in *black*.

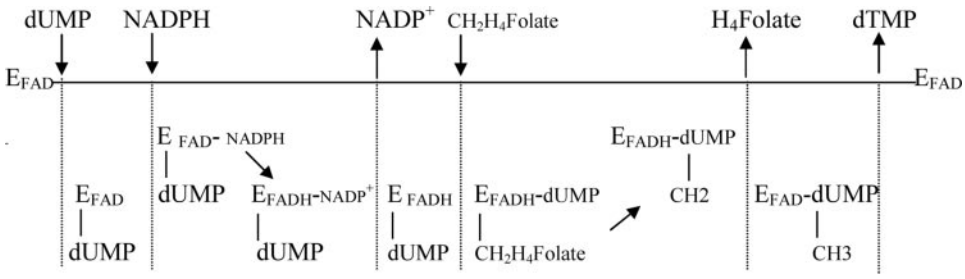

FIGURE 7. **Cleland plot for the proposed catalytic mechanism of ThyX proteins.** Note that the order in which dUMP and NADPH bind and products are released from the active site has not been investigated in detail.

Our site-directed mutagenesis, chemical modification, and structural data have provided new insight into the active site of ThyX proteins. Although our kinetic data indicate formation of a ternary NADPH-dUMP complex (Fig. 7), an earlier study has proposed a ping-pong mechanism implicating the formation of a methyl enzyme intermediate during turnover of *C. trachomatis* ThyX (7). It is of note that we have been unable to detect the proposed covalent intermediate using

either radioactively labeled $^{14}CH_2H_4$folate or mass spectrometric analyses for either PBCV-1 or *C. trachomatis* ThyX proteins (data not shown). The reasons for these experimental discrepancies are currently unknown. However, double-reciprocal plots apparently suggesting a ping-pong mechanism have also been measured for *Lactobacillus casei* ThyA protein (8), although all other kinetic data supported a sequential mechanism. Moreover, the order of substrate binding of ThyA proteins has been reported to depend on buffer composition used in the experiments (1). Additional experimental evidence is required to elucidate the role of the proposed ternary complexes of PBCV-1 ThyX in catalysis.

Acknowledgments—We thank James van Etten and Yuannan Xia for the pVEX plasmid, Yap Boum for help with the NADPH oxidation assays, and Didier Mazel for providing the thymidine auxotroph DH5α strain.

REFERENCES

1. Carreras, C. W., and Santi, D. V. (1995) *Annu. Rev. Biochem.* **64,** 721–762
2. Myllykallio, H., Lipowski, G., Leduc, D., Filee, J., Forterre, P., and Liebl, U. (2002) *Science* **297,** 105–107
3. Mathews, I. I., Deacon, A. M., Canaves, J. M., McMullan, D., Lesley, S. A., Agarwalla, S., and Kuhn, P. (2003) *Structure* (*Camb.*) **11,** 677–690
4. Agrawal, N., Lesley, S. A., Kuhn, P., and Kohen, A. (2004) *Biochemistry* **43,** 10295–10301
5. Gattis, S. G., and Palfey, B. A. (2005) *J. Am. Chem. Soc.* **127,** 832–833
6. Graziani, S., Xia, Y., Gurnon, J. R., Van Etten, J. L., Leduc, D., Skouloubris, S., Myllykallio, H., and Liebl, U. (2004) *J. Biol. Chem.* **279,** 54340–54347
7. Griffin, J., Roshick, C., Iliffe-Lee, E., and McClarty, G. (2005) *J. Biol. Chem.* **280,** 5456–5467
8. Daron, H. H., and Aull, J. L. (1978) *J. Biol. Chem.* **253,** 940–945
9. Lorenson, M. Y., Maley, G. F., and Maley, F. (1967) *J. Biol. Chem.* **242,** 3332–3344
10. Pogolotti, A. L., Jr., Ivanetich, K. M., Sommer, H., and Santi, D. V. (1976) *Biochem. Biophys. Res. Commun.* **70,** 972–978
11. Leduc, D., Graziani, S., Lipowski, G., Marchand, C., Le Marechal, P., Liebl, U., and Myllykallio, H. (2004) *Proc. Natl. Acad. Sci. U. S. A.* **101,** 7252–7257
12. Demarre, G., Guerout, A. M., Matsumoto-Mashimo, C., Rowe-Magnus, D. A., Marliere, P., and Mazel, D. (2005) *Res. Microbiol.* **156,** 245–255
13. Miles, E. W. (1977) *Methods Enzymol.* **47,** 431–442
14. Kabsch, W. (1993) *J. Appl. Crystallogr.* **26,** 795–800
15. Vagin, A., and Teplyakov, A. (1997) *J. Appl. Crystallogr.* **30,** 1022–1025
16. Perrakis, A., Morris, R., and Lamzin, V. S. (1999) *Nat. Struct. Biol.* **6,** 458–463
17. Murshudov, G. N., Vagin, A. A., and Dodson, E. J. (1997) *Acta Crystallogr. Sect. D. Biol. Crystallogr.* **53,** 240–255
18. Roussel, A., and Cambillau, C. (1989) *Silicon Graphics Geometry Partner Directory*, Silicon Graphics, Mountain View, CA
19. Laskowski, R. A., MacArthur, M. W., Moss, D. S., and Thornton, J. M. (1993) *J. Appl. Crystallogr.* **26,** 283–291
20. Sampathkumar, P., Turley, S., Ulmer, J. E., Rhie, H. G., Sibley, C. H., and Hol, W. G. (2005) *J. Mol. Biol.* **352,** 1091–1104
21. Fraaije, M. W., and Mattevi, A. (2000) *Trends Biochem. Sci.* **25,** 126–132
22. Lemaire, M., Schmitter, J.-M., Issakidis, E., Miginiac-Maslow, M., Gadal, P., and Decottignies, P. (1994) *J. Biol. Chem.* **269,** 27291–27296
23. Karplus, P. A., and Schulz, G. E. (1989) *J. Mol. Biol.* **210,** 163–180
24. Hubbard, P. A., Liang, X., Schulz, H., and Kim, J. J. (2003) *J. Biol. Chem.* **278,** 37553–37560
25. Gouet, P., Courcelle, E., Stuart, D. I., and Metoz, F. (1999) *Bioinformatics* **15,** 305–308

Catalytic Mechanism and Structure of Viral Flavin-dependent Thymidylate Synthase ThyX

Sébastien Graziani, Julie Bernauer, Stéphane Skouloubris, Marc Graille, Cong-Zhao Zhou, Christophe Marchand, Paulette Decottignies, Herman van Tilbeurgh, Hannu Myllykallio and Ursula Liebl

J. Biol. Chem. 2006, 281:24048-24057.
doi: 10.1074/jbc.M600745200 originally published online May 17, 2006
